Journal of Power Sources 267 (2014) 98–103

Contents lists available at ScienceDirect

Journal of Power Sources

journal homepage: www.elsevier.com/locate/jpowsour

A seeding method to change primary particle of oriented attachment network titanium dioxide for dye-sensitized solar cells

Ping-Lin Kuo*, Chun-Hou Liao

Department of Chemical Engineering, National Cheng Kung University, Tainan 70101, Taiwan, ROC

HIGHLIGHTS

- The seeding method was used to improve thermal stability and thermal stress.
- The OA S2 has high surface area, lower R_w and perfectly aligned lattice.
- A higher efficiency was achieved by OA S2 as compared with commercial JGC 18NRT.

ARTICLE INFO

Article history:
Received 28 February 2014
Received in revised form
21 April 2014
Accepted 7 May 2014
Available online 20 May 2014

Keywords:
Oriented attachment
Dye-sensitized solar cells
Thermal stability
Thermal stress
Titanium dioxide

ABSTRACT

In this paper, we use seeding methods to improve crystal thermal stability and thermal stress by oriented attachment (OA) particles as seeds. The OA S2 synthesized by repeating two times the seed process has pure anatase phase even if was calcined and high surface area (113.2 $m^2\ g^{-1}$). Further, the lattice images of OA S2 obtains from oriented attachment mechanism showed perfect alignment in grain orientation and no grain boundary appears between the necking particles. The films of OA S2 after calcination at 500 °C is homogeneous without cavities over large area. The photovoltaic performance of dye-sensitized solar cells made of OA S2 exhibits higher J_{SC} and FF than the devices made of JGC 18NRT. The reason for the higher J_{SC} can be attributed to the high surface area and pure anatase phase. The OA S2 shows the lower R_w (charge transport resistance) than the JGC 18NRT. It is confirmed that the OA S2 film has the capability of higher electron transmission due to oriented attachment structure, so it displays low internal resistance and results in higher FF. A higher light-to-electricity power conversion efficiency of 6.10% is achieved by applying the OA S2 as compared with JGC 18NRT (5.85%).

1. Introduction

The dye-sensitized solar cell (DSSC) is one of the most promising low-cost, high-efficiency, and environmentally friendly solar cells [1]. The DSSC is composed of the high-surface-area TiO_2 film on a conducting glass substrate, high absorption efficiency sensitized-dye, I^-/I_3^- redox electrolyte solution, and counter electrode with platinum coating. The dynamics competition process in DSSC for the initial events of electron injection and dye regeneration leading to photo-induced charge separation, which occurs in the femto-second to nanosecond time scale. However, the electron transport in the TiO_2 film and interfacial electron recombination on the TiO_2 surface with I_3^- are in milliseconds or even seconds domain [2]. Therefore electron transport and interfacial recombination are the key factors affecting the efficiency.

In order to accelerate electron transport and decrease interfacial recombination, 1D nanostructure TiO_2 (nanotubes [3–5], nanorods [6], and nanowires [7,8]) are prepared for DSCs. It was anticipated that they would have a single crystalline structure to facilitate incremental electron transportation in the photoelectrode and less surface defects for reducing interfacial recombination on the TiO_2 surface. However, compared with nanoparticles, 1D structures possess lower surface-area that affects dye adsorption and then decrease current density and conversion efficiency.

In order to maintain hight surface-area for increasing electron transport and decreasing interfacial recombination, the Adachi's group synthesizes the network structure of single-crystal-like TiO_2 [9]. The TiO_2 grow by the "oriented attachment" mechanism resulted in that the orientations of crystals of fused nanoparticles with completely aligned orientation. The OA TiO_2 possess high

* Corresponding author.
E-mail address: plkuo@mail.ncku.edu.tw (P.-L. Kuo).

http://dx.doi.org/10.1016/j.jpowsour.2014.05.049
0378-7753/

surface-area due to small particle size (2–5 nm) and accelerate electron transport as a result of perfectly aligned lattice. A high light-to-electricity power conversion yield of 9.3% was achieved by applying OA as the titania thin film of dye-sensitized solar cells. But the OA TiO_2 exists two problem: (1) after calcination at 500 °C the anatase phase TiO_2 change to rutile phase; (2) the OA film obtained from terpineol base paste is easy to crack after calcination.

The seeding method is easy method to change material morphology, Kuang group use seeding method to increase TiO_2 nanowire arrays surface area [10,11]. In this paper, we use seeding methods to improve crystal thermal stability and thermal stress resulted from the increased particle size. After calcination the OA S2 film present pure anatase phase and on crack over large area. An enhancement of conversion efficiency based on that the OA S2 (6.10%) is achieved as compared with JGC 18NRT (5.85%).

In this paper, we use seeding methods to improve crystal thermal stability and thermal stress resulted from the increased particle size. After calcination the OA S2 film present pure anatase phase and on crack over large area. An enhancement of conversion efficiency based on that the OA S2 (6.10%) is achieved as compared with JGC 18NRT (5.85%).

2. Experimental

2.1. Preparation of oriented attachment TiO_2

Commercially available titanium isopropoxide (TIPO, 97%) and acetylacetone (AA, 99.8%) were used as received. The oriented attachment TiO_2 was synthesized according to the work of Adachi's group [9]. TIPO was mixed with AA and adjusted to pH 2, then stirred one day at 50 °C. The final solution was placed in a Teflon-lined autoclave and aged at 120 °C for three days. The network TiO_2 was designated as OA. The OA TiO_2 as seed particles again was mixed the precursor-solution and then placed in a Teflon-lined autoclave, lastly aged at 120 °C for three days. The network TiO_2 was designated as OA S1. The OA S2 and OA S3 were synthesized by repeating the seed process.

2.2. Device fabrication

For the preparation of the nanoporous TiO_2 layers with OA and OA S1–S3, the viscous slurries were prepared by the following procedure [12]. The TiO_2 was dispersed in ethanol and then mixed with terpineol and ethyl cellulose. After removing the ethanol with a rotary-evaporator, the final paste was obtained. The FTO glass plates were cleaned by surfactant, acetone and isopropanol and subsequently immersed into a 40 mM $TiCl_4$ aqueous solution at 70 °C for 30 min, lastly washed with water. Then the OA and OA S1–S3 TiO_2 paste and commercial paste JGC 18NRT (JGC Catalysts and Chemicals Ltd., Japan.) were coated onto the FTO substrate using the screen-printing method. The coated films were baked at 150 °C for 30 min and then sintered at 450 °C for 15 min and at 500 °C for 15 min. After calcination, the TiO_2 film was treated with 40 mM $TiCl_4$ solution as described above. The films were sintered again at 450 °C for 30 min. After cooling down to 80 °C, the TiO_2 electrodes were sensitized by immersing into dye solutions of 0.5 mM N719 dye (Solaronix) in acetonitrile and tertiary butanol (in the volume ratio of 1:1) at room temperature for 16 h. The dye-covered TiO_2 films and the Pt counter electrodes were assembled into sealed sandwich-type cells by heating with hot melt sealing foil (SX1170-25, 25 μm thickness, Solaronix) used as spacers between the electrodes. A hole was made by a sandblasting drill on the counter electrode, allowing the internal space between the two electrodes to be filled with electrolyte solution (0.1 M LiI, 0.6 M DMPII, 0.05 M I_2, and 0.5 M TBP in 3-Methoxypropionitirle, MPN) using a vacuum backfilling system. After electrolyte filling, the hole was sealed with a thin glass sheet.

2.3. TiO_2 characterization and photovoltaic

Characterization of the TiO_2 are performed with transmission electron microscopy (TEM) at 80 kV (JEOL, JEM-1200EX), high resolution-transmission electron microscopy (HR-TEM) (FEI Tecnai G2), X-ray diffraction (XRD) at 40 kV and 30 mA (Rigakue, RINT2000), and isotherm of nitrogen adsorption at 77 k (Micromerit ASAP 2020), to get TiO_2 particles size, crystalline structures, surface area and pore size distribution respectively. Characterizations of the TiO_2 electrodes are measured by field emission scanning electron microscope (FE-SEM) at 10 kV (JEOL, JSM-6700F) to get TiO_2 films morphology.

Photocurrent–voltage measurements were performed using an solar simulator (SAN-EI, Model:XES-301S, Japan). The electrochemical impedance spectroscopy (EIS) measurements in this study were carried out by applying bias modulation near the open circuit condition (Voc) [13]. EIS measurements of cells were recorded in a frequency range from 0.05 Hz to 1 MHz with an ac amplitude of 10 mV. The active area of the dye-coated TiO_2 film was 0.16 cm^2.

3. Results and discussion

In this study, the system used acetylacetone (AA) not only as a stabilizer for TIPO to reduce the hydrolysis rate of the alkoxide, but also as a shape controller to specifically adsorb on the particle surfaces. In accordance with Adachi's group, the TiO_2 has characteristic crystal growth by the oriented attachment mechanism and forms a network of single-crystal-like anatase nanowires [9]. The network TiO_2 (designated as OA) was composed of fused nanoparticles with diameters of only 3–5 nm as shown in Fig. 1(a). Fig. 1(b) presents the SEM image of surface morphology OA film obtained from coating of terpineol base paste, followed by calcination at 500 °C for 30 min. The high-magnification SEM image (Fig. 1(b) inset) demonstrates that most of the particles are connected with each other and form a network of nanoparticles. However, the OA film of the low-magnification SEM image showed cracks due to the thermal stress after calcinations. In addition, the XRD pattern of the OA particle shows the existence of anatase and rutile phase as a result of calcinations (Fig. 1(c)).

Seeding methods reacting at 120 °C were used to improve crystal thermal stability and to release thermal stress by OA particles as seeds. Fig. 2(b)–(d) shows the TEM images of TiO_2 with three different seeding times, labeled as OA S1, OA S2, and OA S3. The OA S1~S3 seem to be the network structure with coating grown on the OA particles. As the seeding times increased, the network TiO_2 particle size increased (Fig. 2(b)–(d)). On the other hand, in order to understand the effect of the growth temperature on the morphology of the seeding particles, the different seeding temperature are compared in Fig. 2 (b) and (e). The TiO_2 precursors at 120 °C migrated into the OA as seeds, where nucleation occurs at particles surfaces as shown in Fig. 3. The OA S1 particles size grew from 3 to 5 nm to 6–8 nm. There are a lot of small nanoparticles adhering to the surface of OA particles when the growth temperature was decreased to 80 °C.

The XRD patterns of the OA and OA S1–S3 calcined at 500 °C for 30 min are shown in Fig. 4. For the OA S2 and OA S3, the figure shows that the peaks at 25.2° and 38.5° (TiO_2 anatase, JCPDS No. 21-1272) correspond to the planes (101) and (004) respectively, and confirms the pure anatase phase without any contamination of the other TiO_2 polymorphs. However, the OA S1 reveals the weak peaks of rutile (110) at $2\theta = 27.5°$ (TiO_2 rutile, JCPDS No. 21-1276),

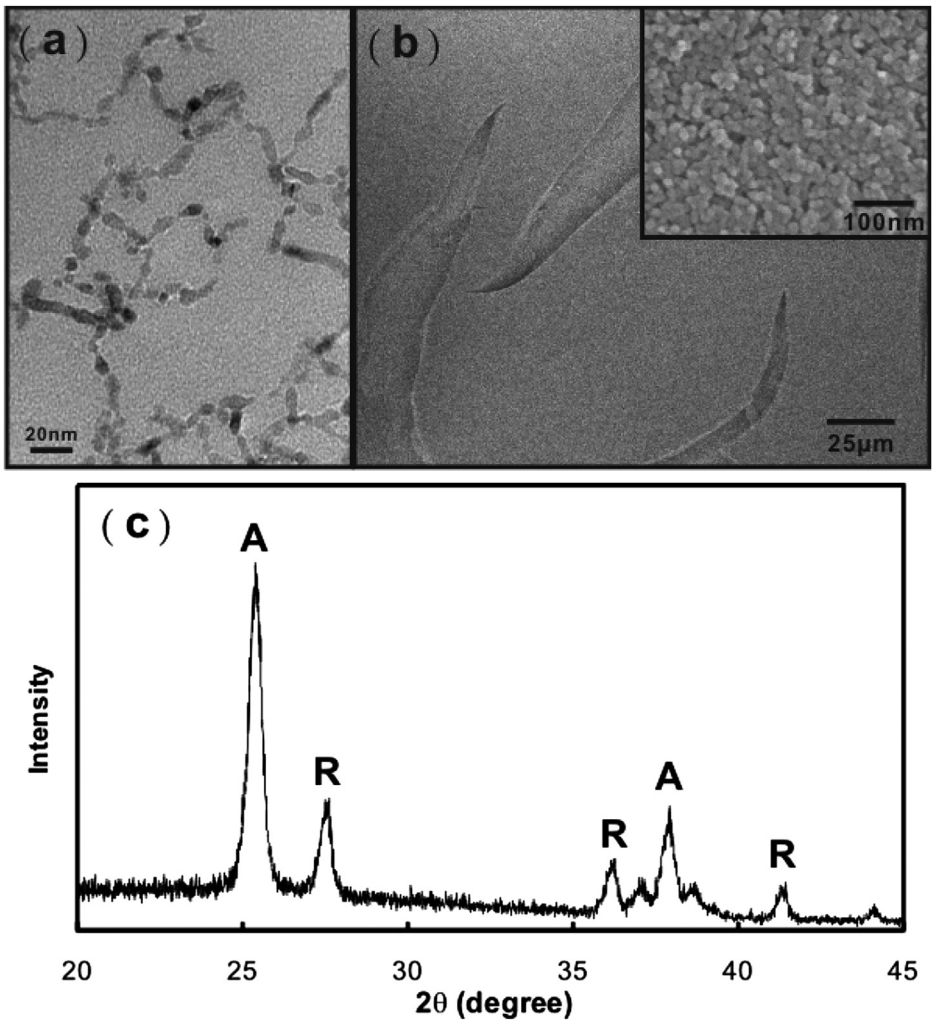

Fig. 1. (a) TEM image, (b) SEM image, and (c) XRD pattern for OA.

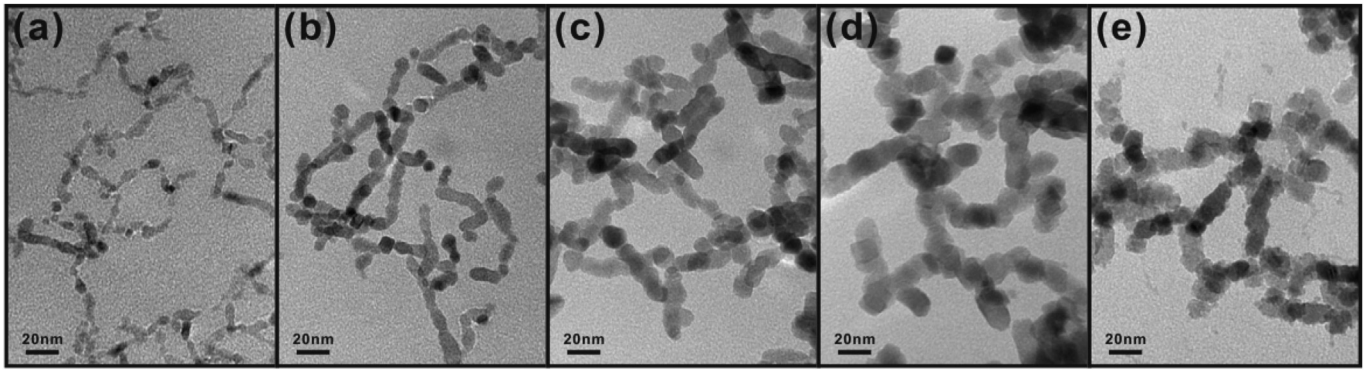

Fig. 2. TEM images of the samples:(a) OA, (b) OA S1, (c) OA S2, (d) OA S3 for 120 °C and (e) OA S1 for 80 °C.

indicating that it still contains some rutile phase [14]. It is well known that the electron mobility of anatase is higher than rutile [15]. So the anatase form of TiO_2 is important for preparing efficient dye-sensitized solar cells [16]. The following experiments only focus on OA S1–S3.

Further structural analyses of the OA S1–S3 are performed using high-resolution TEM. The HR-TEM image (Fig. 5) of the network TiO_2 clearly shows the lattice spacing is 0.35 nm which corresponds to the lattice spacing of (101) plane in the anatase phase. For the OA S1 and OA S2 the lattice images aligned perfectly, and no grain boundary appeared between the necking particles. This result shows that the network TiO_2 is mainly obtained from the oriented attachment mechanism. With the increase of the seeding times for the network TiO_2, the grain boundaries would gradually appear between the necking particles. The OA S3 displays imperfect grain alignment of the lattice images.

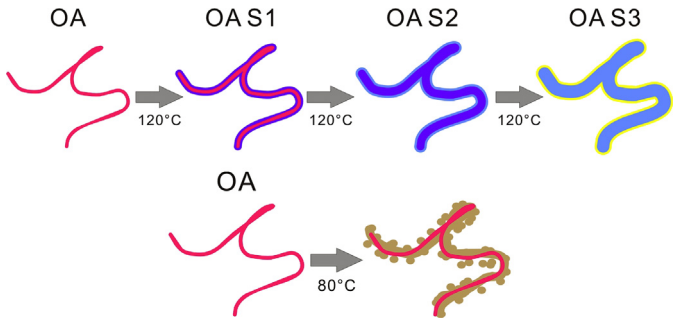

Fig. 3. Schematic illustration for the preparation of the seeding TiO_2 in 120 °C and 80 °C.

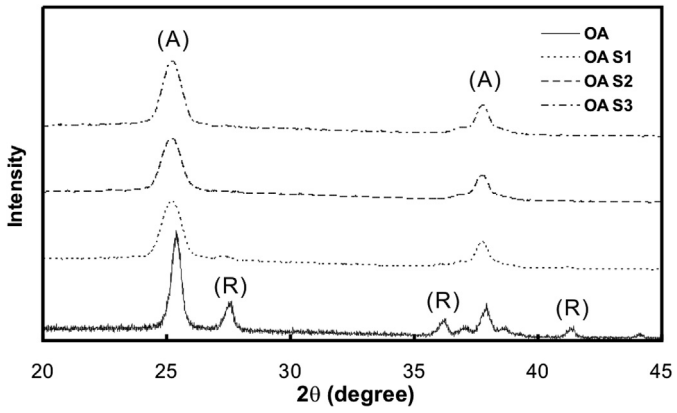

Fig. 4. XRD pattern for OA, OA S1, OA S2, and OA S3 after calcination.

To estimate the amount of dye adsorbed on the photoelectrode, the N_2 adsorption–desorption measurement was applied to analyze the properties of the OA S1–S3. The nitrogen adsorption–desorption isotherm of the OA S1–S3 taken from a TiO_2 film in the DSC system calcined at 500 °C for 30 min are shown in Fig. 6. The isotherms of the OA S1~S3 are of type IV according to the IUPAC classification, which is a characteristic of the mesoporous compound. The hysteresis loop of type H1 is observed in the case of the OA S1, which is of compacted smaller particles arranged in regular array and hence had narrow distributions of pore size. With the increase of the network particles, the hysteresis loop of OA S2–S3 is change from type H1 to type H3, which is observed with aggregates of secondary particles giving rise to slit-shaped pores [17,18]. The BET (Brunauer–Emmett–Teller) specific surface area of the OA S1 is 169.4 $m^2\ g^{-1}$ and the pore distribution ranges from 2 to 15 nm with a BJH (Barrett–Joyner–Halenda) pore size of 8.6 nm as can be seen in Fig. 6. The OA S2 and OA S3 has BET specific surface area of 113.2 $m^2\ g^{-1}$ and 89.8 $m^2\ g^{-1}$ respectively and are lower than that of OA S1. The BJH pore diameter of the OA S2 and OA S3, which are 12.8 nm and 20.1 nm respectively, are higher than that of OA S1. It is well known that the large pore size can help electrolyte diffusion.

The detailed morphology for the top surface of TiO_2 films is investigated by using field emission scanning electron microscopy (SEM). As shown in Fig. 7(e)–(h), all the films after calcination at 500 °C for 30 min are very homogeneous without cavities over large area. Fig. 7(a) shows a high magnification SEM image of the OA S1 film which shows more compact structures with small void spaces. With the increase of the seeding times, the OA S2 and OA S3 films show larger void spaces due to greater particle size (Fig. 7(b)–(c)). The results correspond with the BJH analysis. In comparison with the OA S2 and OA S3 film, the commercial TiO_2 (JGC 18NRT) film displays smaller void spaces.

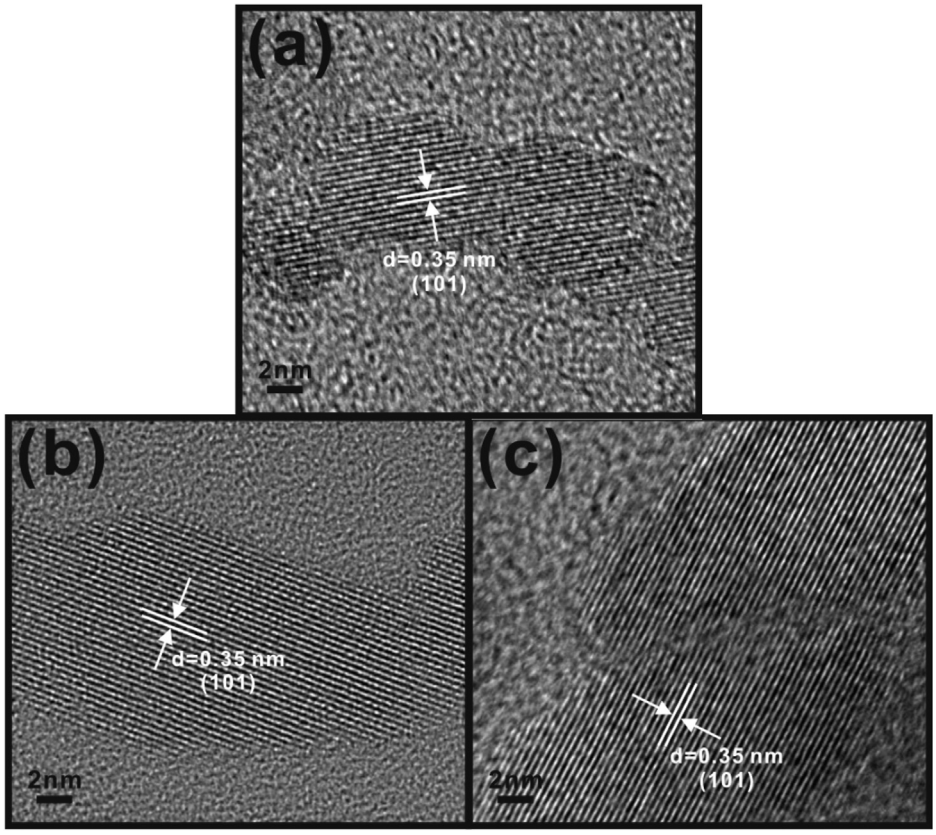

Fig. 5. AEM images for (a) OA S1, (b) OA S2, and (c) OA S3.

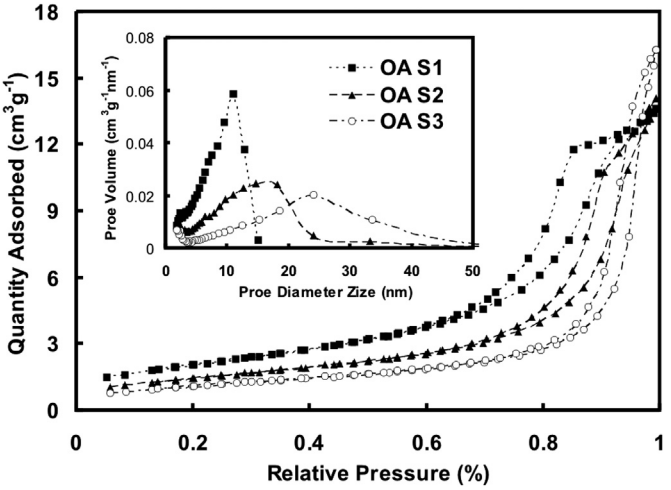

Fig. 6. Nitrogen adsorption isotherm pattern and the pore size distribution of the OA S1, OA S2 and OA S3.

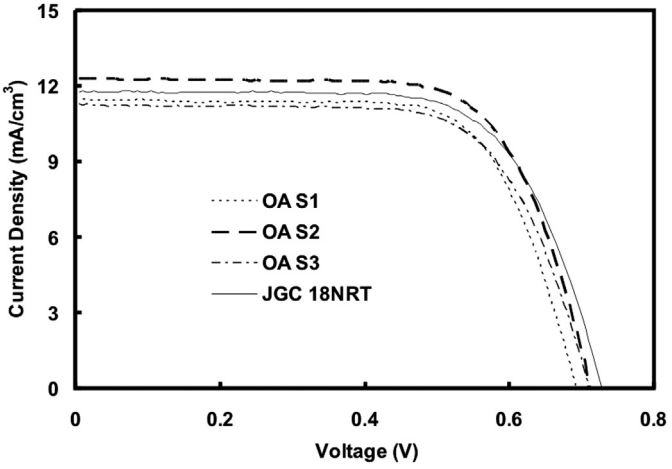

Fig. 8. *I–V* curves of the DSC assembled with OA S1, OA S2, OA S3, and JGC 18NRT.

As mentioned above, the OA S1 possesses highest surface area, but it contains some rutile phase that was proved to affect electron transmission [14]. The OA S3 has lowest surface area and displays that the lattice images do not aligned perfectly. However, the OA S2 possesses higher surface area, pure anatase phase and perfectly aligned lattice. The OA S2 is expected to display higher light-to-electric power conversion efficiency for DSSC.

The performances in dye solar cells of the OA S1–S3 and JGC 18NRT that are evaluated under 1 Sun AM 1.5 simulated sunlight are shown in Fig. 8 and Table 1. The OA S2 exhibits higher J_{SC} and FF than the other TiO_2. The reason for the higher J_{SC} can be attributed to the high surface area. The OA S1 has highest surface area, but it contains small amount of rutile. The rutile existence will affect electron transmission. The FF is determined by the internal resistance of the cell. The resistances source comes from conducting glass, ion diffusion in the electrode-pore, and electron conductivity in the electrode and counter electrode. The TiO_2 films of OA S1–S3 are characterized by their capability of higher electron transmission due to oriented attachment structure, so they displays low internal resistance that results in higher FF. An enhancement of light-to-electric power conversion efficiency can be observed based on that the OA S2 (6.10%) achieved comparable results with JGC 18NRT (5.85%).

Table 1
Characterization and photovoltaic test summary of the four TiO_2 photoanodes.

Films/DSSCs	J_{SC} (mA cm^{-2})	V_{oc} (V)	FF (%)	η (%)	S_{BET} (m^2 g^{-1})
OA S1	11.4	0.69	0.70	5.57	169
OA S2	12.3	0.71	0.70	6.10	113
OA S3	11.2	0.71	0.69	5.47	89
JGC 18NRT	11.7	0.73	0.68	5.85	73

In order to investigate the electron transport and charge recombination property in TiO_2 film electrodes, the electrochemical impedance spectroscopy (EIS) are employed. Fig. 9 shows the Nyquist plots of the EIS of OA S2 and JGC 18NRT. The Nyquist plots exhibit three semicircles including : (1) the low frequency semicircle which is attributed to diffusion resistance of I^-/I_3^- in the electrolyte [13,19–22]; (2) the central arc which is influenced by (i) charge transport resistance (R_w) ascribed to the accumulation/transport of the injected electrons in TiO_2 film and (ii) charge recombination resistance (R_k) occurred when the electron crosses either the TiO_2/redox electrolyte interface or the TiO_2/FTO interface

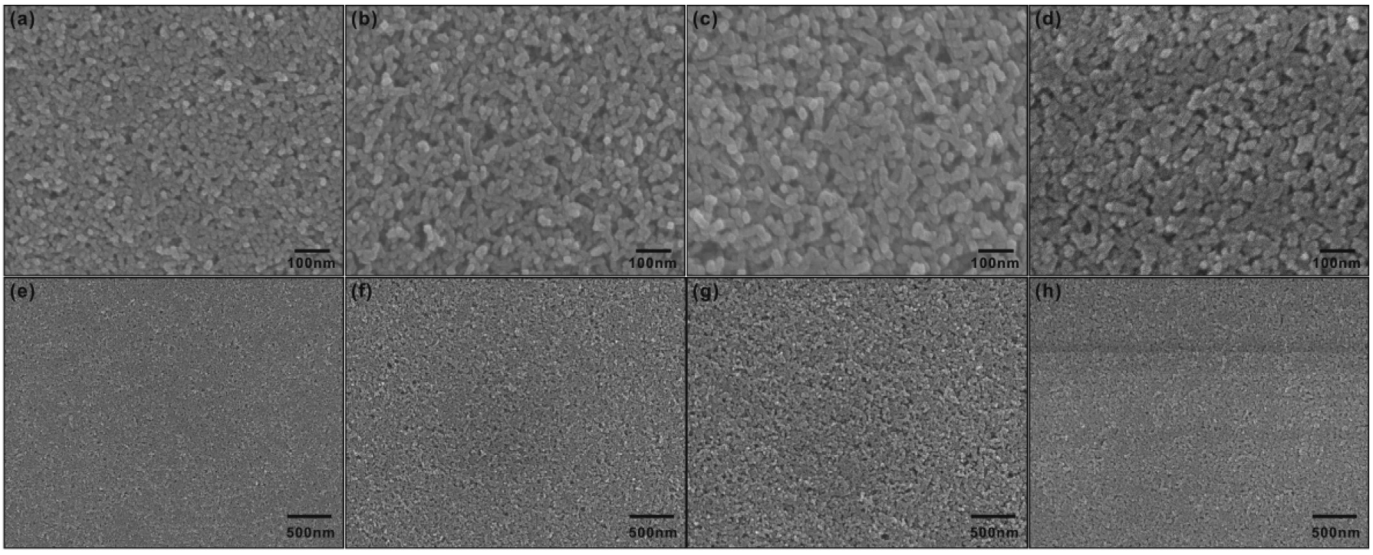

Fig. 7. SEM images for (a and e) OA S1, (b and f) OA S2, (c and g) OA S3, and (d and h) JGC 18NRT.

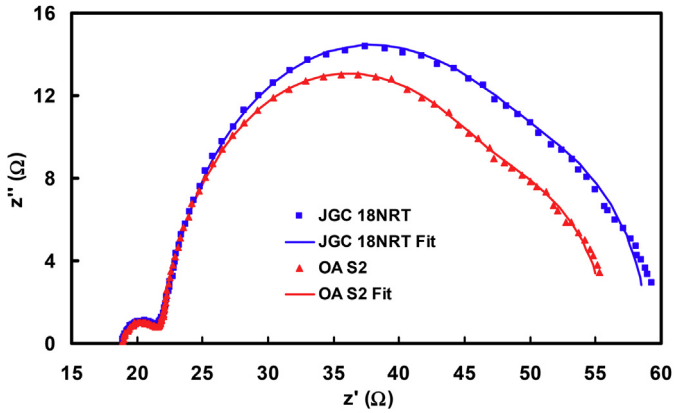

Fig. 9. Electrochemical impedance spectroscopy (EIS) for dye-sensitized solar cells with OA S2 and JGC 18NRT, respectively.

Table 2
Properties of DSSC determined by electrochemical impedance spectroscopy (EIS) measurements.

	τ_{eff} (s)	R_k (Ω)	R_w (Ω)
JGC 18NRT	0.16	25.62	2.53
OA S2	0.20	23.68	2.39

[13,19–23]; (3) the high frequency semicircle which is assigned to the electron transfer at the Pt counter electrode [13].

From Fig. 9, a series of TiO_2 properties (R_w, τ_{eff} and R_k) for OA S2 and the reference JGC 18NRT were acquired by fitting the central arc in Nyquist plots of EIS, as shown in Table 2. The R_w in the OA S2 is 2.39 Ω, which is lower than the JGC 18NRT, indicating that the oriented attachment structure lowered the charge transport resistance by reducing grain boundaries. The charge transport resistance, which could dominate the FF, will be reduced by the oriented attachment structure and resulted in increase of FF. The result coincided with the DSSC performances (Table 1), where the OA S2 displayed higher FF than the JGC 18NRT. For the τ_{eff} value, the OA S2 (0.20 s) is higher than that of JGC 18NRT (0.16 s), showing that effective lifetime of electron in OA S2 electrode is longer than JGC 18NRT electrode. This can be attributed to the oriented attachment structure. However, the R_k value is 23.68 Ω for the OA S2 and 25.62 Ω for the JGC 18NRT, showing that the recombination reaction is not effectively prevented by the OA S2. A small difference in V_{oc} observed in Table 1 is in accordance with R_k value for OA S2 and JGC 18NRT.

4. Conclusions

In this study, seeding methods was used to improve crystal thermal stability and to release thermal stress. The OA S2 has high surface area (113.2 $m^2\ g^{-1}$) and perfectly aligned lattice. Further calcination at 500 °C, the OA S2 still displays pure anatase phase and the OA S2 filmes are homogeneous without cavities over large area. The performance of OA S2 exhibits higher J_{SC} due to high surface area and pure anatase phase. Furthermore, the OA S2 showed lower R_w (charge transport resistance) than the JGC 18NRT and confirmed that the electron transport in the OA S2 film was accelerated due to oriented attachment structure. The OA S2 displays low internal resistance that results in higher FF. A higher light-to-electricity power conversion yield of 6.10% was achieved by applying the OA S2 as compared with JGC 18NRT (5.85%).

References

[1] B. O'Regan, M. Gratzel, Nature 353 (1991) 737–740.
[2] M. Gratzel, Chem. Lett. 34 (2005) 8–13.
[3] G.K. Mor, K. Shankar, M. Paulose, O.K. Varghese, C.A. Grimes, Nano Lett. 6 (2006) 215–218.
[4] K. Zhu, N.R. Neale, A. Miedaner, A.J. Frank, Nano Lett. 7 (2007) 69–74.
[5] D. Kim, A. Ghicov, S.P. Albu, P. Schmuki, J. Am. Chem. Soc. 130 (2008) 16454.
[6] B. Liu, E.S. Aydil, J. Am. Chem. Soc. 131 (2009) 3985–3990.
[7] J.J. Wu, G.R. Chen, C.C. Lu, W.T. Wu, J.S. Chen, Nanotechnology 19 (2008).
[8] J.K. Oh, J.K. Lee, H.S. Kim, S.B. Han, K.W. Park, Chem. Mat. 22 (2010) 1114–1118.
[9] M. Adachi, Y. Murata, J. Takao, J.T. Jiu, M. Sakamoto, F.M. Wang, J. Am. Chem. Soc. 126 (2004) 14943–14949.
[10] W.-Q. Wu, Y.-F. Xu, C.-Y. Su, D.-B. Kuang, Energy Environ. Sci. 7 (2014) 644–649.
[11] J.-Y. Liao, B.-X. Lei, H.-Y. Chen, D.-B. Kuang, C.-Y. Su, Energy Environ. Sci. 5 (2012) 5750–5757.
[12] S. Ito, P. Chen, P. Comte, M.K. Nazeeruddin, P. Liska, P. Péchy, M. Grätzel, Prog. Photovolt. Res. Appl. 15 (2007) 603–612.
[13] M. Adachi, M. Sakamoto, J. Jiu, Y. Ogata, S. Isoda, J. Phys. Chem. B 110 (2006) 13872–13880.
[14] L.M. Nikolic, L. Radonjic, V.V. Srdic, Ceram. Int. 31 (2005) 261–266.
[15] U. Diebold, Surf. Sci. Rep. 48 (2003) 53–229.
[16] N.G. Park, J. van de Lagemaat, A.J. Frank, J. Phys. Chem. B 104 (2000) 8989–8994.
[17] K.S.W. Sing, Pure Appl. Chem. 54 (1982) 2201–2218.
[18] K.S.W. Sing, D.H. Everett, R.A.W. Haul, L. Moscou, R.A. Pierotti, J. Rouquerol, T. Siemieniewska, Pure Appl. Chem. 57 (1985) 603–619.
[19] H. Xu, X. Tao, D.-T. Wang, Y.-Z. Zheng, J.-F. Chen, Electrochim. Acta 55 (2010) 2280–2285.
[20] L. Han, N. Koide, Y. Chiba, T. Mitate, Appl. Phys. Lett. 84 (2004) 2433–2435.
[21] T. Hoshikawa, M. Yamada, R. Kikuchi, K. Eguchi, J. Electrochem. Soc. 152 (2005) E68–E73.
[22] T. Hoshikawa, T. Ikebe, R. Kikuchi, K. Eguchi, Electrochim. Acta 51 (2006) 5286–5294.
[23] A. Hauch, A. Georg, Electrochim. Acta 46 (2001) 3457–3466.